Bidirectional reflectance measurements over a micrometric surface area using a goniospectrophotometer

Dipanjana Saha, Lou Gevaux, Jeppe Revall Frisvad, Gael Obein

Review of Scientific Instruments

RESEARCH ARTICLE | MAY 23 2024

Bidirectional reflectance measurements over a micrometric surface area using a goniospectrophotometer

Dipanjana Saha ; Lou Gevaux ; Jeppe Revall Frisvad ; Gael Obein

Rev. Sci. Instrum. 95, 055114 (2024)
https://doi.org/10.1063/5.0193490

AIP Publishing

Review of Scientific Instruments ARTICLE pubs.aip.org/aip/rsi

Bidirectional reflectance measurements over a micrometric surface area using a goniospectrophotometer

Cite as: Rev. Sci. Instrum. 95, 055114 (2024); doi: 10.1063/5.0193490
Submitted: 22 December 2023 • Accepted: 9 May 2024 •
Published Online: 23 May 2024

Dipanjana Saha,[1,a)] Lou Gevaux,[1] Jeppe Revall Frisvad,[2] and Gael Obein[1]

AFFILIATIONS

[1] LNE-CNAM, Department of Radiometry and Photometry, 61 rue du Landy, 93210 La Plaine St Denis, France
[2] Department of Applied Mathematics and Computer Science, Technical University of Denmark, Richard Petersens Plads, 324, 160, 2800 Kongens Lyngby, Denmark

[a)] **Author to whom correspondence should be addressed:** dipanjana.saha@lecnam.net

ABSTRACT

The increasing use of a spatially varying bidirectional reflectance distribution function (svBRDF) to describe the appearance of an object raises the important question of how BRDF values change when measured on a small scale. For this reason, we present a new goniospectrophotometer with the ability to measure the BRDF at the micrometer scale (μBRDF). The instrument produces BRDF measurements with a measurement surface diameter of 31 μm. This device is designed to aid in the extension of the BRDF metrological scale from centimeter to micrometer size. We support the credibility of our μBRDF measurements using a specially made test sample with uniform diffuse white dots on a uniform black background, measuring its bidirectional reflectance in one geometrical configuration at many spatial locations. This sample can easily be modeled using a few unknown parameters. The agreement between our measurements and the model demonstrates the credibility of the measurement technique.

INTRODUCTION

People measure different optical quantities, such as reflectance and transmittance, to assess the appearance of a material. However, the appearance of a material is also strongly influenced by the distance at which it is observed. Therefore, the geometrical conditions under which those quantities are captured should be chosen carefully. When we look at a piece of cloth from a distance of a few meters, it does not have the same appearance as when we look at it from a distance of a few centimeters. When we look from afar, we can see the entire pattern of the cloth. Yet, when we look closely, we can see the yarn, the fibers of the textile materials, the weave pattern, and the texture.

The demand for measuring the reflectance of materials as if observed at a short distance is increasing. One reason for this is that virtual prototyping is rapidly growing in popularity for engineering or marketing purposes in a variety of industries, including automobiles, cosmetics, and textiles. In virtual prototyping, physically based rendering is obtained by using models that assign the optical properties of the material at the micrometer scale to render the appearance of the material at a larger scale,[1,2] but the values used at the micrometer scale are extrapolated and never measured.

In 3D and 2.5D printing, researchers are improving the optical qualities of printing materials and technologies to make printed objects look more like their digital counterparts. There is a rising demand in this field for knowledge concerning material optical properties at a very small scale, i.e., the scale of a few voxels, which means tens of micrometers, in order to improve the reproduction quality.[2]

To characterize the appearance of a material, we need to measure its bidirectional reflectance distribution function (BRDF). Judd[3] and Nicodemus[4] introduced the quantity and did the first measurements. Since that time, different goniospectrophotometers have been developed at National Metrological Institutes to measure BRDF with optical settings (spectral bandwidth, angular resolution, angular step, etc.) that allow the characterization of color,[5,6] goniochromatism,[7,8] gloss,[9,10] sparkle,[11–14] and translucency.[10,15,16]

Substantial efforts are currently being made to improve the quality and stability of these instruments.[17] However, no metrologically validated system exists to improve the spatial resolution of BRDF measurements, allowing the characterization of the optical properties of very small objects.

To meet this need, a new goniospectrophotometer has been developed at LNE-Cnam (the French-designated institute for radiometry, photometry, and spectrophotometry) to perform microscale BRDF measurements (μBRDF), meaning traceable BRDF measurements performed on submillimeter or micrometer surfaces, in order to assist the computer rendering community and 3D printer manufacturers in validating their multiscale models.

In this study, we focus on the dimensional aspect of the measurement surface and propose evaluating our bidirectional reflectance measurement system in a single geometric configuration, which can then be generalized to the measurement of μBRDF over the whole hemisphere. This paper describes the experimental facility, settings, and validation of the system.

DEFINITION AND OBJECTIVES

The geometric parameters involved in the measurement of a BRDF are shown in Fig. 1. Orthogonal unit vectors **x**, **y**, and **z** describe the sample coordinate system. The direction of illumination **i** and observation **r** are, respectively, defined in this coordinate system by the azimuthal angles $\varphi_\mathbf{i}$ and $\varphi_\mathbf{r}$ and the zenith angles $\theta_\mathbf{i}$ and $\theta_\mathbf{r}$. The variables $\Omega_\mathbf{i}$ and $\Omega_\mathbf{r}$ denote the solid angles of illumination and collection around the directions **i** and **r**. The measured surface has an area called A. A measurement is performed at a wavelength λ with a spectral bandwidth $\Delta\lambda$. The BRDF[18] is defined as the quotient of the surface differential element of radiance in the direction **r** to the differential element of the irradiance on the medium along the direction **i** and has units of inverse steradians (sr^{-1}).

As a ratio of infinitesimals, the BRDF cannot be measured directly. However, when the solid angles $\Omega_\mathbf{i}$ and $\Omega_\mathbf{r}$ that are defined by the setup optical design are negligible according to the angular variations of the BRDF of the sample, the BRDF can be expressed as a flux ratio with a geometrical factor.[19] For measurements performed in an under-illumination configuration, the BRDF equation is

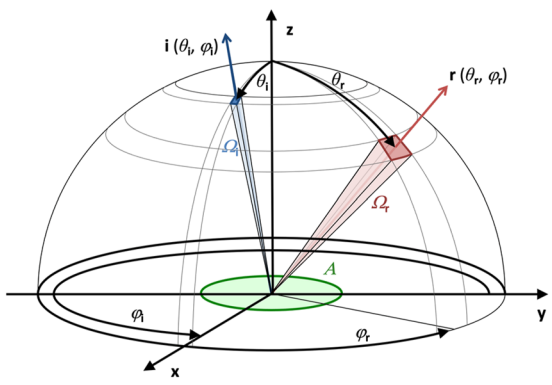

FIG. 1. Geometrical description and notations.

$$f(\mathbf{i},\mathbf{r},\lambda) = \frac{\Phi_\mathbf{r}(\mathbf{i},\mathbf{r},\lambda)}{\Phi_\mathbf{i}(\mathbf{i},\lambda)\cos\theta_\mathbf{r}\Omega_\mathbf{r}}, \quad (1)$$

where λ is the wavelength, $\Phi_\mathbf{i}$ is the incident flux from direction **i**, $\Phi_\mathbf{r}$ is the reflected flux in direction **r**, and $\Omega_\mathbf{r}$ is the solid angle around **r**.

To perform a BRDF measurement, we need a facility able to orient both the illumination and the observation directions relative to the sample anywhere in the hemisphere above it. The incoming and reflected fluxes must be measured at a desired wavelength, and the solid angle of collection ($\Omega_\mathbf{r}$) must be known.

For our μBRDF setup, we target the following settings:

- visible spectrum, 380 nm < λ < 780 nm,
- circular measurement area A with a diameter of Ø < 100 μm,
- angular resolution $\Delta\theta < 2°$,
- spectral bandwidth $\Delta\lambda$ < 3 nm,
- any directions of the hemisphere up to zenith angles <80°.

DESCRIPTION OF THE SYSTEM

General design

The goniospectrophotometer for measuring μBRDF consists of a rotating illumination system embedded on a 1 m diameter ring, a 6-axis robot arm as a sample holder, and an immobile detection system (Fig. 2). The μBRDF setup shares the same mechanical elements with our existing primary BRDF system, which is the national reference BRDF measurement setup, and with CONDOR, which can measure BRDF with high angular resolution (0.015°).[20,21]

The goniospectrophotometer has been designed to perform absolute BRDF measurements, with the capability to measure both the incident flux from the illumination system and the reflectance flux from the sample. The robot arm is an RV 12S from Mitsubishi. It allows us to translate the sample along the **x**, **y**, and **z** axes in order to center it on the goniospectrophotometer. It also allows the rotation of the sample around **x**, **y**, and **z**. A fourth rotation is provided by the ring bearing the illumination system. With four rotations, all angular configurations for illumination **i** and observation **r** are accessible.[22] For in-plane BRDF measurement, only rotation around **y** on the robot and around **d** on the ring is needed. For out-of-plane configurations, four rotations are required. The angular steps of the stepper motors for the robot and the ring are 0.01°.

Illumination system

For illumination, an EQ99 Laser Driven Light Source (LDLS, Hamamatsu) is used. The power spectral density of the LDLS is close to that of a Xenon arc, which is adapted to our objective to cover the visible spectral range. Our main motivation to use this type of source is that the radiant exitance is high and, compared to a Xenon arc, the light plasma dot is more stable in space and smaller in size. The diameter of the plasma is around 200 μm. To achieve an illumination area on the sample with a diameter below 100 μm, we developed an imaging optical system with a magnification γ of 0.1 that images the LDLS plasma on the sample. This source is shared with CNAM's BSSRDF setup and is described in detail in Ref. 16.

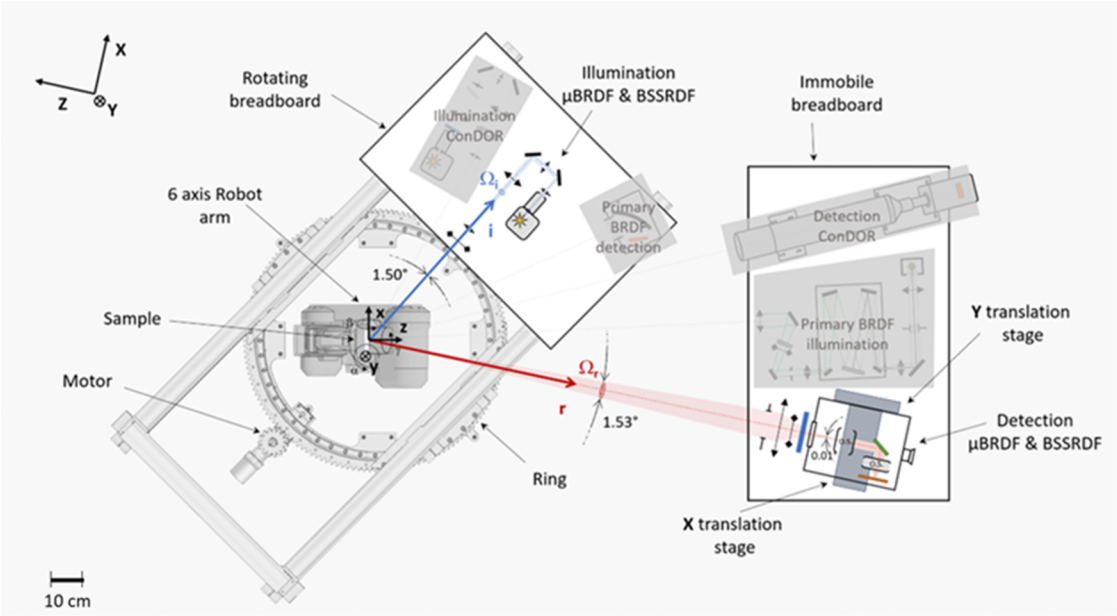

FIG. 2. General implementation of the μBRDF gonio. The system shares the ring, the robot arm, and the optical tables with two existing BRDF setups in our facility: "Primary BRDF" and "ConDOR." The illumination is on the rotating breadboard (blue). The detection is on the fixed optical table (red). The rotation of the table is done with a large, motorized ring. The three other rotations are done at the sample level, with the robot arm.

Optical design

As the illumination system is mounted on a breadboard on the rotating ring around the robot arm, there is a gap of 580 mm between the last optical component of the illumination system and the sample. We designed a two-lens system (Fig. 3) to respect this 580 mm gap and keep the system compact enough to fit on the breadboard.

The convergence angle has been set to 1.5° by calculating the exit pupil (EP) diameter. This allows us to maximize the flux in the system while keeping our objective of an angular resolution below 2°.

The adopted solution consists of a light beam source of diameter 200 μm ($\varnothing_p$), a 1-in. diameter diverging achromatic doublet of focal length −50 mm (L1), and a 1-in. diameter converging achromatic doublet of focal length 250 mm (L2). The inter-distance between the lenses is 428 mm. With this system, the image of the plasma is focused at 580 mm after L2. The exit pupil (EP) is adjusted with a diaphragm placed 28 mm in front of L2. The diameter of the diaphragm is set to 12.7 mm to obtain a convergence of 1.5°, and the expected diameter of the image of the source beam ($\varnothing_p'$) is 20 μm.

The full system has been folded to fit in a rectangular area of 300 × 600 mm^2.

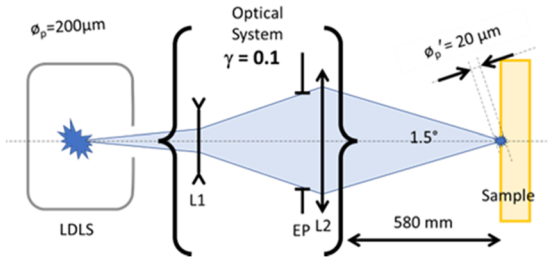

FIG. 3. Optical drawing of the illumination system showing the input parameters and the constraints linked to the mechanical design.

Characterization of the illumination beam

To optimize the focus of the optical system and characterize the illumination beam on the sample plane, a scanning slit beam-scanner from OPHIR NanoScan was used. The beam shape shown in Fig. 4 is the best focus of the beam that we were able to produce.

The power distribution of the plasma inside the LDLS, combined with the spherical and chromatic aberration of the optical components, determines the shape of the power distribution of the beam. At the foot of the beam, we can see in Fig. 4(a) a figure of diffraction with a "cross" shape, which is not a characteristic of the beam but comes from the limits of the OPHIR NanoScan device.

Based on these measurements, we assume a Gaussian shape. For both the **x** and **y**-axes, the Gaussian curves that best fit the beam power profile were estimated using the 85% upper values of the measured data. Results are reported in Table I and shown in Fig. 4(c) for the **x**-axis. For both axes, the correlation between the Gaussian and the measured data is good (>0.996).

In the following, we will consider that our beam has a Gaussian shape with a standard deviation (σ) of 13.5 μm, which is the average σ along the **x** and **y** axes. The average full width at half maximum (FWHM) is 31.3 μm.

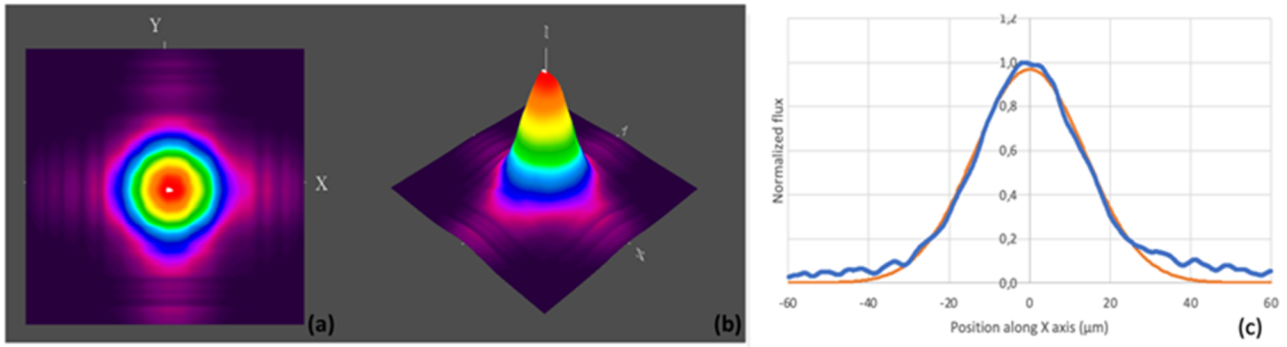

FIG. 4. Beam shape measured by OPHIR NanoScan, (a) 2D view. (b) 3D view. (c) Normalized beam profile along the **x**-axis (blue curve) and Gaussian fit (orange curve).

TABLE I. Dimensions of the illumination beam and standard deviation of the Gaussian fit.

	Measurement	Gaussian fit	
	FWHM (μm)	Standard deviation (μm)	Corr. coeff.
x	31.0	13.3	0.996
y	31.6	13.7	0.998

Detection system

As the illumination beam is broadband, the detector must be spectrally selective. The detection system used to measure the incident and reflected flux is a CS2000 spectroradiometer from Konica–Minolta. The CS2000 has a spectral resolution of $\Delta\lambda = 0.9$ nm that satisfies our objective ($\Delta\lambda < 3$ nm). It can measure low radiant fluxes, which is appropriate in our situation because our beam is tiny and consequently has a low flux. However, the CS2000 aperture and measurement area do not meet the objectives listed in Sec. II. Consequently, the optics of the CS2000 were replaced by a custom optical system, whose specifications and optical design are described below. This detection system is also shared with CNAM's BSSRDF setup.[16]

Field of view and aperture specifications

The distance between the spectroradiometer and the sample plane is roughly 1700 mm and is constrained by the general design of the goniospectrophotometer (see Fig. 2). At that distance, the smallest measuring angle of the CS2000 gives a field of view (FoV) of 3 mm. This is much larger than our 31.3 µm illuminated area. To avoid a contribution from the non-illuminated area (due to ambient stray light) so significant that it would drastically decrease our signal-to-noise ratio, we selected a FoV of 300 µm. With such a FoV, the observation area overfills the illuminated area on the sample for zenith angles of up to 80° without vignetting, while keeping the ratio between illuminated and observed areas acceptable.

To maintain a satisfactory level of flux, the aperture angle of our detection system must be as large as possible. However, from another side, the aperture angle defines the angular resolution of the setup and, thus, must be kept below 2°. In addition, because of the 1.7 m distance between the sample and the detection unit, we must keep the aperture angle small to avoid having a very large entrance pupil that would require even larger optical components. We selected a circular entrance pupil with a diameter of 45 mm. This gives an aperture angle of 1.53°, meets the objective of $\Delta\theta < 2°$, is compatible with the incident beam aperture (1.5°), and allows us to use 3 in. lenses that are easy to find in catalogs.

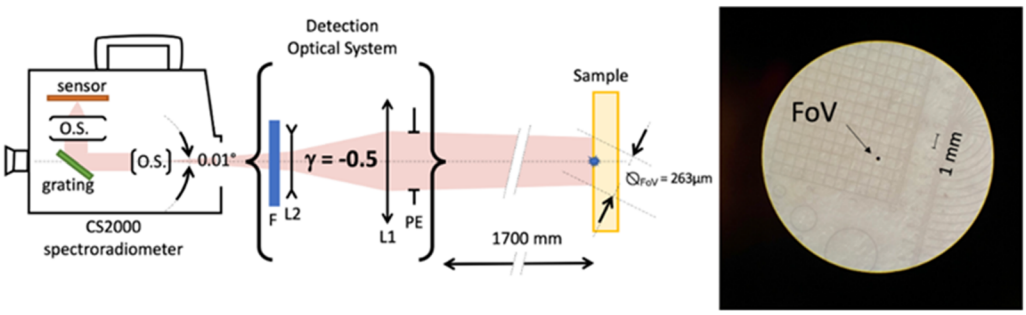

FIG. 5. Left: Optical drawing of the detection system with the two lenses, allowing us to reduce the FoV of the CS2000 by a factor of 10 while keeping the focal distance at 1700 mm. Right: Picture of the FoV on a micrometric ruler, seen in the ocular of the spectroradiometer.

Optical design

We replaced the commercial optics of the CS2000 with a custom optical system (Fig. 5, left), comprising a 3-in. converging achromatic doublet of focal length 150 mm (L1) and a 1-in. diameter diverging achromatic doublet of focal length −50 mm (L2). A filter (F), originally part of the commercial optics, is placed after L2 because the CS2000 spectral calibration was performed with this filter. The entrance pupil of the system is a diaphragm (PE) placed before L1, which controls the aperture of the system and, thus, the collection solid angle $\Omega_{\mathbf{r}}$. The distance between L1 and L2 is 10 cm, and the distance between L2 and the image plane is 20.5 cm. The magnification is $\gamma = 0.5$. As the location of the image plane in the CS2000 is not precisely known, the position of the CS2000 is adjusted so that the object is in focus in the ocular of the CS2000. The diameter of the area measured by the CS2000, evaluated using a micrometric ruler, is $\text{Ø}_{\text{FoV}} = 263 \pm 5$ µm (Fig. 5, right).

The study carried out in Ref. 16 with the same illumination and detection systems has shown that a correction factor, attributed to stray light in the detection's optical system, was required for incident light measurement. The value of this correction factor is $k_{SL} = 0.714$ (±0.014). This factor has been applied to the experimental measurements presented in the following sections.

VALIDATION

To validate our µBRDF goniospectrophotometer, the use of a calibrated diffuse reflectance standard is not possible. White diffuse reflectance standards such as sintered PTFE (commercially known as Spectralon), which scatter light in volume, exhibit translucency at the micrometer scale.[16] Metallic reflective diffusers, which scatter light on the surface, feature a rough reflecting surface with a roughness in the order of a hundred micrometers obtained by sandblasting with coarse grind (e.g., 120 grit). For these reasons, the reflectance properties of these standards at the micrometer scale are different from their calibration values measured at the centimeter scale. Thus, a direct comparison between our µBRDF measurements and the calibration values is not relevant.

Furthermore, we would like to validate not only the value of the measured BRDF but also the size of the measurement area, which is the area that can be measured independently. This is not possible with a large and uniform sample, because such a sample does not allow us to determine whether the measurement results at the micrometric scale are affected by the material surrounding the measurement area. Instead, we need to use a sample exhibiting a known pattern with uniform material properties on areas of micrometric size. The setup characterization presented in this section relies on studying our ability to measure the transition between two areas of different optical properties.

To validate the setup, we propose to scan the BRDF of a sample featuring alternating high and low levels of reflectance along a linear direction (Fig. 6, top). In this situation, the theoretical result is a square function, and the measurement result should be the convolution of the square function with our Gaussian beam (Fig. 6, bottom). Experimentally confirming that this is the case will enable us to validate the µBRDF measurement setup.

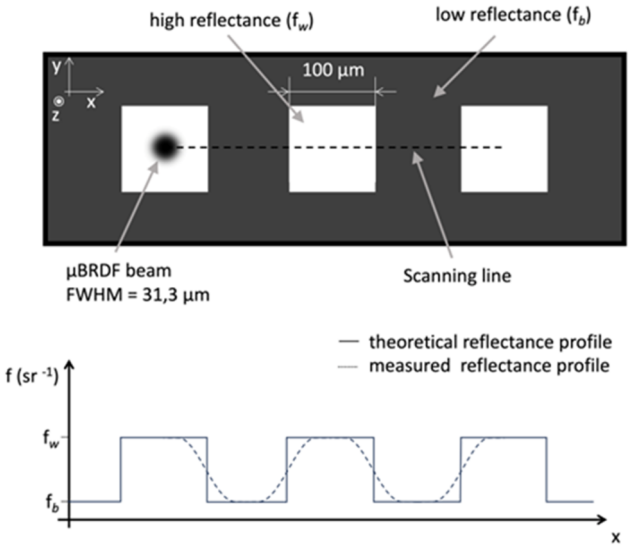

FIG. 6. Principles of validation. Top: Drawing of a test sample with alternate white and black patches at a sub-millimetric scale. The BRDF of the sample is measured along the scanning line with the µBRDF beam. Bottom: Plain line: Theoretical reflectance along the scanning line. Dash line: Expected measured reflectance, being the convolution between the µBRDF beam and theoretical reflectance.

Test samples

The produced samples are presented in Fig. 7. We used circular patches because they were easier to manufacture than squares, and we arranged them in grids of dots to have more scanning line options. Concretely, samples consist of glossy black Plexiglass (PMMA) of 1 mm thickness and size 5 × 5 cm^2, in which cylindrical holes have been drilled with an automatic drilling machine. The diameters of the drill bits are 100 µm, 300 µm, 500 µm, and 1 mm. The holes have been filled with a white resin that consists of polyurethane (PU) resin and titanium dioxide (TiO_2) pigments added in a 4:1 weight ratio.[23] After the resin had dried, the samples were polished with grit 280 sandpaper to obtain a smooth, matte, diffuse, and isotropic surface. For the 100 µm drill bit, it was not possible to produce a grid of dots with our existing drilling system

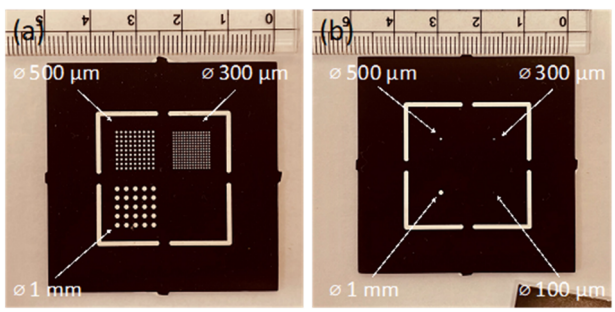

FIG. 7. Picture of the samples produced for the validation of the µBRDF gonio. (a) Dot grids with different sizes. (b) Single dots with different sizes.

TABLE II. Design details of the samples.

Size of dots, diameter			Space between two dots (center to center)	
Nominal value (μm)	Average value (μm)	Number of dots per grid	Nominal value (μm)	Average value (μm)
1000	1029 ± 9	5 × 5	2000	1980 ± 30
500	498 ± 4	9 × 9	1000	995 ± 10
300	334 ± 5	14 × 14	600	610 ± 15
100	105 ± 5	⋯	⋯	⋯

because the size was too small. The specifications of the samples are reported in Table II.

The sample with single dots (Fig. 7, right) was developed with the purpose of making μBRDF comparisons in the future with other institutes. Only the smallest single dot (Ø = 100 μm) has been used in the present study.

Experimental measurements

We carried out bidirectional reflectance measurements on our dot grid samples in the geometry ($\theta_\mathbf{i} = 0^\circ$, $\varphi_\mathbf{i} = 0^\circ$; $\theta_\mathbf{r} = 14^\circ$, and $\varphi_\mathbf{r} = 180^\circ$). Following the definition of BRDF given in Eq. (1), BRDF values are calculated from the raw measurements of the radiance incident on the sample L_s and its associated dark $L_{s,k}$, the radiance reflected on the sample $L_\mathbf{r}$ and its associated dark $L_{\mathbf{r},k}$, the geometrical parameters $\Omega_\mathbf{r}$ and $\theta_\mathbf{r}$, as well as the stray light correction factor k_{SL}. The measurement equation is

$$f(\mathbf{i},\mathbf{r}) = k_{SL}\frac{L_\mathbf{r} - L_{\mathbf{r},k}}{L_s - L_{s,k}}\frac{1}{\cos\,\theta_\mathbf{r}\Omega_\mathbf{r}}. \tag{2}$$

The spectroradiometers provide spectral data, allowing us to compute BRDF for each wavelength of the spectral range. However, to maximize the signal-to-noise ratio of the measurements, we decided to compute luminance by integrating the spectral radiance multiplied by the V(λ) function, at the cost of spectral resolution. This allows us to use the stray light correction factor determined in the same spectral conditions.

We performed BRDF measurements along the scanning line (Fig. 6). The total number of measurements varies between 30 and 135 points, depending on the dot sizes (see Table III). Between two repetitions, the sample is unmounted and realigned. The alignment errors are estimated to be less than 0.3° for the roll, pitch, and yaw of the sample and less than 20 μm in the **x** and **y** directions. It takes ~5 min to get one measurement point.

The results are reported in Fig. 8 (left column). For dot sizes of 1000, 500, and 300 μm, the BRDF values reach a plateau around 0.30 sr^{-1} for the white dot and around 0.05 sr^{-1} for the black part. For the 100 μm dot, the plateau is not reached. We observe a noise of ~0.05 sr^{-1} between each repetition, which represents more than 15% of the signal in the case of the white part.

Measurement analysis

The experimental results illustrated in Fig. 8 show noise that represents more than 15% of the signal for the white part. To better understand the sources of noise, we propose a simple uncertainty analysis. The measurement uncertainty is evaluated by combining the standard uncertainties u_X associated with each variable X in Eq. (3),[24]

$$\frac{u_f}{f} = \sqrt{\left(\frac{u_{k_{SL}}}{k_{SL}}\right)^2 + \left(\frac{u_{\Omega_\mathbf{r}}}{\Omega_\mathbf{r}}\right)^2 + \left(\frac{u_{L_s}}{L_s}\right)^2 + \frac{u_{L_\mathbf{r}}^2 + u_{L_{\mathbf{r},k}}^2}{\left(u_{L_\mathbf{r}} - u_{L_{\mathbf{r},k}}\right)^2} + \left(\tan\left(\theta_\mathbf{r}\right)u_{\theta_\mathbf{r}}\right)^2}. \tag{3}$$

The relative uncertainty of the correction factor k_{SL} has been estimated at 1.9% in Ref. 16. The uncertainty of the solid angle is calculated from the uncertainty of the distance between the sample and the aperture of the detection system (0.02%) and the uncertainty of the aperture diameter (1%). Its relative value is 2%. The uncertainty of the polar angle $\theta_\mathbf{r}$ is estimated at 0.3°, which contributes to the overall uncertainty of 1.3×10^{-3}.

The relative uncertainty of the source measurement L_s is evaluated at 2% from several independent readings of the signal. This value accounts for the stability of the source and for the alignment of the detector in front of the source by the operator, which strongly impacts the measurement. Finally, the uncertainty of the reflectance

TABLE III. Measurement details.

Dot size (μm)	Number of dots measured	Measurement points	Measurement steps (μm)	Repetition
100	1	30	15	4
300	3.5	80	25	3
500	2	84	25	4
1000	2	135	30	3

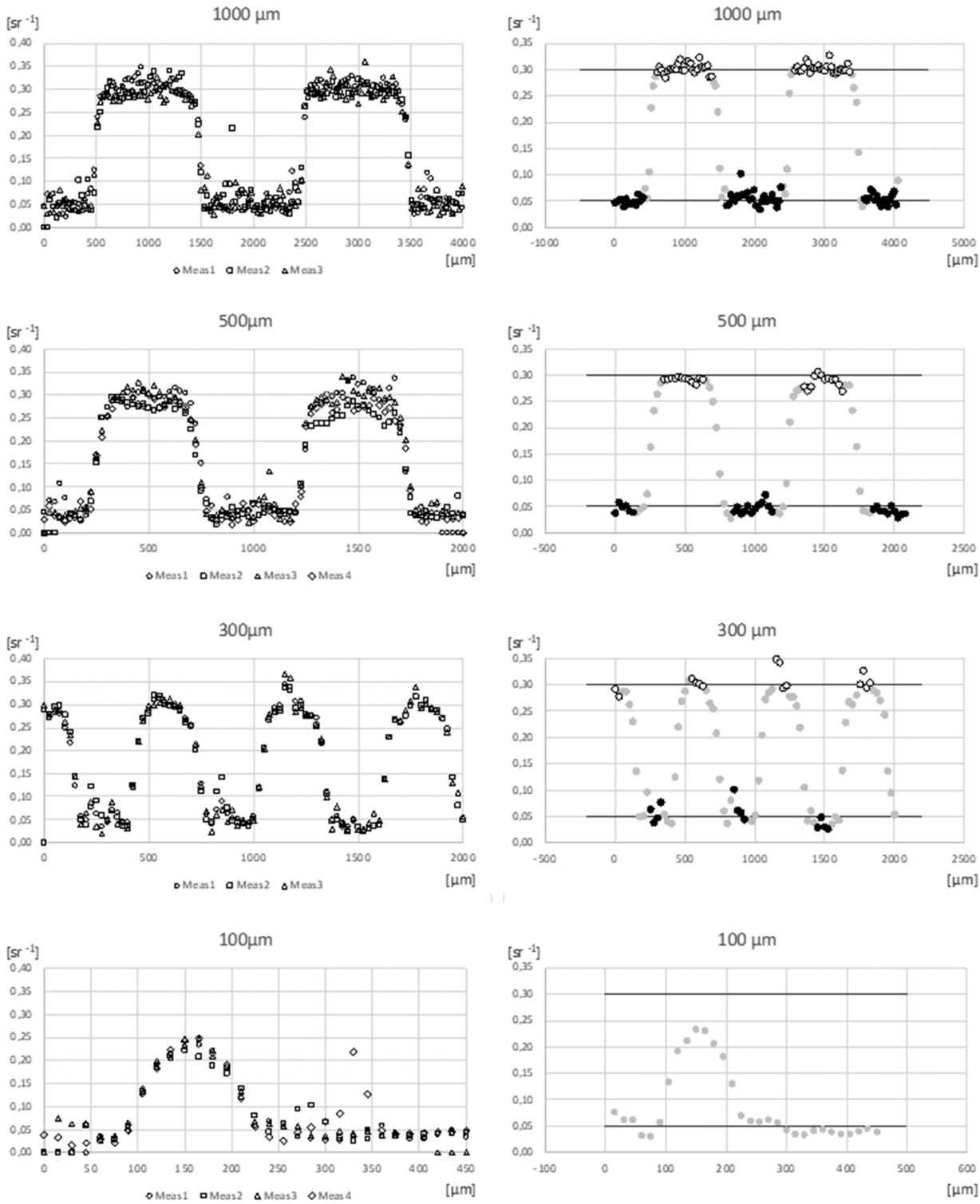

FIG. 8. Bidirectional reflectance (sr^{-1}) according to the measurement position (μm) of sample grid 1000, 500, 300, and 100 µm in the geometry ($\theta_i = 0°$, $\varphi_i = 0°$; $\theta_r = 14°$, and $\varphi_r = 180°$). Left column: Superposition of the 3 or 4 repetitions. Right column: Average BRDF with identification of the points used in the calculation of f_W (white circles) and f_B (black circles). Gray circles are not involved in these calculations.

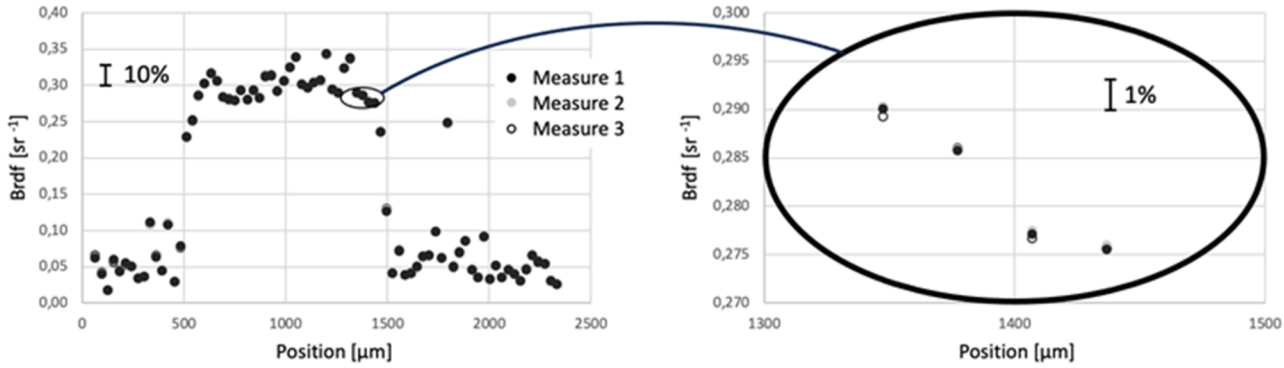

FIG. 9. Repeatability test of the gonio. Measurement done on a 1000 µm diameter dot.

radiance and its associated dark signal $L_r - L_{r,k}$ is evaluated through a repeatability measurement on a 1000 µm diameter dot, with three consecutive measurements for each position along the profile. The results, plotted in Fig. 9, give us a repeatability of 0.25%.

The combined standard uncertainty of the bidirectional reflectance measurement is 3.4%, calculated using Eq. (3). This uncertainty is significantly lower than the 15% noise observed between the different repetitions, which shows that these high fluctuations do not correspond to noise from the measurement instrument itself. Our hypothesis is that this noise mainly comes from random scratches on the surface of the sample. To get homogeneous and isotropic samples, as mentioned earlier, we polished the surface with grit 280 sandpaper. However, even if the sample surface looks homogeneous on visual inspection, it is likely that, at the micrometer scale, the scratches made by the sandpaper are not negligible and cause these high fluctuations between the different repetitions. The similar BRDF fluctuations observed for the white and black areas support this hypothesis, as the random scratches are similar in both areas.

Nevertheless, because of its origin, we think that this noise can be assumed to be random. We, therefore, decided to adopt as the experimental results the average value of the measurement repetitions. These values are plotted in Fig. 8 (right column) for each dot size.

The bidirectional reflectance values f_W and f_B of the white resin and black substrate are assessed by computing the average of the measurement points that belong to each plateau for cases 1000, 500, and 300 µm. The case of 100 µm has been excluded because the plateau has not been reached. We consider a point to belong to the plateau when it is located more than 100 µm away from the middle of the transition between the black and white zones. The points selected for computing both constants are highlighted in Fig. 8, right column. The adopted values are reported in Table IV.

The reproducibility calculated on the averaged data is 0.5% for the bidirectional reflectance of the white part, which is lower than the standard combined uncertainty evaluated above (3.4%). It shows that by averaging a large number of measurement points, we are able to minimize the impact of the random scratches on the surface and retrieve experimental BRDF values.

Sample's BRDF model

The measurements of the bi-material sample are modeled by the convolution of a Gaussian function representing the illumination beam with a periodic rectangular function that represents the BRDF of the sample along the scanning line. The rectangular function has a period of 2 times the size of the dots and varies between two plateaus, f_W and f_B, representing the BRDF of the white and black parts, respectively. The model can be written as follows:

$$\hat{f}_X(x) = \mathcal{G}(x,\sigma) \otimes \left[(f_W - f_B) \sum_{i=-\infty}^{\infty} \mathrm{rect}\left(\frac{x - x_0}{X} + 2i - 1 \right) + f_B \right], \tag{4}$$

where

- f_W is the BRDF of the white resin,
- f_B is the BRDF of the black substrate,
- $\mathcal{G}$ is the Gaussian function,
- σ is the standard deviation of the Gaussian illumination beam,
- rect is the rectangular function,
- x_0 is the abscissa offset,
- X is the diameter of the dot.

The model has four unknowns: f_W, f_B, σ, and x_0. The BRDF values f_W and f_B and the standard deviation σ are assumed to be independent of the dot size.

The BRDF values have been calculated above using the measurement points on the plateaus. To estimate the values of σ and x_0, the shape and position of the transitions between each plateau

TABLE IV. Determination of f_W and f_B.

	f_B	f_W
No. of points	97	92
Average (sr^{-1})	0.0507	0.2992
Stand dev (sr^{-1})	0.0130	0.0126
Reproducibility (sr^{-1})	0.0014	0.0014

TABLE V. Optimized values for the s and x0 parameters.

x_0				
Dots 1000 μm	Dots 500 μm	Dots 300 μm	Dots 100 μm	σ
−16.1 μm	−12.3 μm	−12.4 μm	7.7 μm	26.7 μm

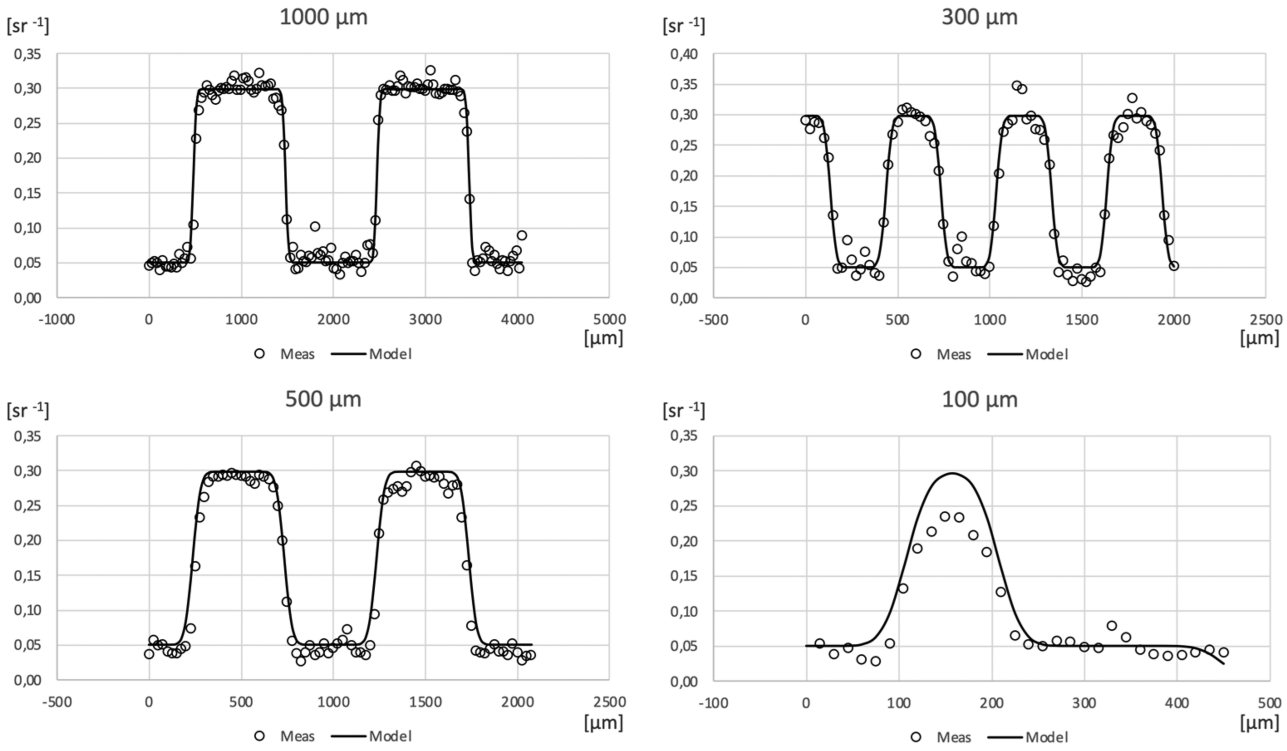

FIG. 10. Measurements and model along the scanning line for the four different dot sizes. Circles: measurements, Line: Model using f_B, f_W, σ, and x_0 as input.

are used. The Nelder–Mead simplex search algorithm[25] is applied to optimize the distance between the measurements and model by adjusting the standard deviation of the Gaussian σ and the abscissa offset vector x_0. The best fit is obtained with the values reported in Table V.

The x_0 values are less than 20 μm away from their intended values. This is of the same order of magnitude as the beam size and agrees with our estimated uncertainty in the sample's spatial alignment. The standard deviation of the Gaussian that allows us to best fit the measurements is σ = 26.7 μm. It corresponds to a beam FWHM of 62.9 μm. This is roughly two times higher than the FWHM measured with the beam scanner (31.3 μm). The possible reasons for this discrepancy will be discussed in the next session. In Fig. 10, we plot the measurement points and the reflectance model.

DISCUSSION

Non-homogeneity of the test samples

The first thing we regret is the non-uniformity of our test samples, which did not allow us to assess the equipment's performance as finely as we would like. The samples were polished until they exhibited a matte and isotropic visual appearance. Nevertheless, measurements showed that this polishing was not sufficient. Ultimately, the stability of the measured signals seems good, as we achieve a repeatability of 0.25% when repeating the measurements without moving the sample (see Fig. 9 in Sec. IV D). Unfortunately, the reproducibility is only 15% in our experiment when we remove and realign the sample, due to the non-homogeneity of the sample surface. Averaging over a large number of points allowed us to carry out our validation work, but the results would have been more

robust if the samples had exhibited a more homogeneous surface aspect.

However, this experimental study allowed us to point out that μBRDF measurements, when performed in the configuration we have developed (under-illumination method), must be conducted on samples with low micrometric-scale roughness. If this is not the case, the measurements will reveal defects and exhibit very strong local fluctuations.

Reflectance of the test samples

By averaging the measurements, we obtained $f_W = 0.2992\ \mathrm{sr}^{-1}$ and $f_B = 0.0507\ \mathrm{sr}^{-1}$ for the BRDF of the white dots and the black substrate. To check the order of magnitude of these values, we investigated the optical properties of the materials. The three main constituents of the samples are black PMMA, PU, and TiO_2. We collected the refractive indices of these three materials from the literature. The refractive index of black PMMA is available from Alinejad *et al.*,[26,27] and that of TiO_2 is available from Siefke *et al.*[28] In the case of transparent PU, we consulted the work of Bauer *et al.*[29] for the absorption and the wavelength dependence of the refractive index and set the absolute value of the real part of the refractive index in the visible part of the spectrum to the 1.468 measured by Moffitt *et al.*[23] We note that we almost have an index match between black PMMA ($n_{vis} = 1.466$) and transparent PU in the visible part of the spectrum. This means that scattering at the interface between the white and black materials in our samples is negligible. The white dots consist of PU with TiO_2 pigments added in a 4:1 weight ratio. The densities of the two constituents reveal a TiO_2 volume fraction of 0.058, which means that an assumption of independent scattering of the particles is reasonable. With the (complex) refractive indices and assuming spherical TiO_2 particles of 340 nm diameter,[23] we used the Lorenz–Mie theory[30] to compute the scattering properties of the white dot material. The resulting properties are shown in Fig. 11.

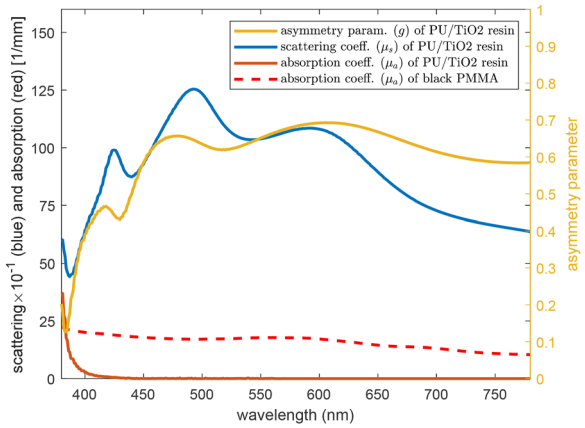

FIG. 11. Absorption of black PMMA and scattering properties of our white resin computed using the volume fraction of TiO_2 in the PU host, the (complex) refractive indices of the constituents, and an assumption of 340 nm diameter spherical TiO_2 particles.

The absorption of the black PMMA is very high (10–20 mm^{-1}), and we may, therefore, reasonably assume that all light entering the black PMMA is absorbed. To model the scattering by the surface, we use the Trowbridge–Reitz microfacet normal distribution[31] and the Torrance–Sparrow BRDF model.[32] For a roughness in this model of 0.089, the reflectance matches our measured value, $f_B = 0.0507\ \mathrm{sr}^{-1}$. This roughness value is in the same range as semi glossy dark paint (reported by Trowbridge and Reitz[31] to have roughness between 0.05 and 0.1), which in terms of roughness seems like a material surface that we can reasonably compare our sandpaper-polished black PMMA surface with.

The estimated optical properties of the white resin indicate that scattering in this resin is high in the visible range, and the roughness of the sample exhibits surface scattering as well. Using Monte Carlo ray tracing to solve the radiative transfer equation[33] with the microfacet surface model also used for the black PMMA as the boundary condition,[32,34] we computed a spectrum of bidirectional reflectances for our selected configuration ($\theta_i = 0°$, $\theta_r = 14°$). We used the optical properties in Fig. 11 as input and the same roughness as for the black PMMA. Due to the particle content of the white resin, its surface roughness could arguably have been set a bit higher, which would lead to slightly larger simulated bidirectional reflectances as our configuration is of the specular peak. An inner product of the spectrum of simulated bidirectional reflectances and the visual sensitivity curve (as done in our measurements) resulted in $f_W = 0.2672\ \mathrm{sr}^{-1}$. Although not a perfect match, this is not too far from the measured value, $f_W = 0.2992\ \mathrm{sr}^{-1}$.

FWHM of the illumination beam

The convolution model described by Eq. (4), used in our validation, has the advantage of depending on very few parameters: f_B, f_W, and σ (with x_0 being an offset). It adequately represents what happens when we scan a line on our test samples for all spot sizes, as indicated by the rather high correlation values between the measurements and the convolution-based model presented in Table VI.

The simulations performed above using a hypothetical sample's optical properties show that the order of magnitude of the reflectance parameters (f_B and f_W) is correct. However, the estimated beam FWHM of 62.9 μm is twice as wide as the measurement obtained with the beam scanner (Fig. 4). Light subsurface scattering in the resin is a potential explanation for this discrepancy between the two values, as the model does not account for the material's translucency.

If we look at a surface patch of white resin measuring less than a square millimeter illuminated by our white beam, the beam appears larger due to subsurface scattering as compared with the

TABLE VI. Correlation coefficient for measurement and modeled data.

Sample	Correlation coefficient
100 μm dots	0.984
300 μm dots	0.987
500 μm dots	0.992
1000 μm dots	0.993

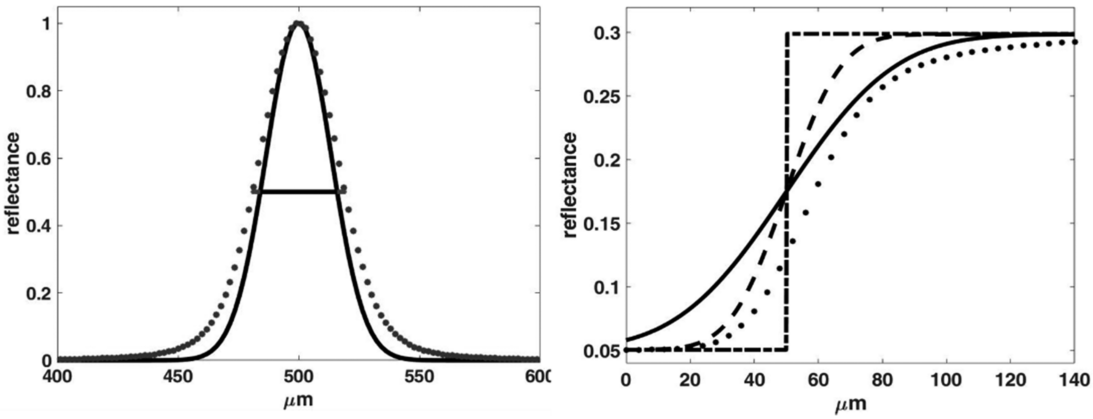

FIG. 12. Results of the Monte Carlo ray tracing simulation carried out at 550 nm for a normal incidence and an observation at 14°. Left: Normalized Gaussian illumination beam (solid curve) and normalized simulated reflectance profile (dotted curve), which features a FWHM of 39.1 μm. Right: Expected reflectance profile for the beam moving across an edge (represented by the irregular dashed curve) between black PMMA and white resin. The regular dashed curve is what our convolution model predicts if using the beam measured with the beam scanner (FWHM = 31.3 μm), the dotted curve is the expected profile from our ray tracing simulation when using the same beam, and the solid curve is fit to the experimental data (FWHM = 62.9 μm). Due to subsurface scattering, the measurements are closer to the Monte Carlo simulation, which has a reflectance profile with a different shape. To best fit the experimental data, the model, therefore, estimates a much wider beam than was actually used.

beam spread measured with the beam scanner. It is, therefore, very likely that the translucency of the white resin is not entirely negligible on a micrometric scale, even though the samples were designed to minimize it.

To evaluate the spread of the beam that we can expect for our white dot samples, we use the optical properties reported in Fig. 11 to perform a ray tracing simulation over a 1 mm^2 patch. Selecting a 550 nm wavelength, we simulated the spatially resolved reflectance due to our beam at a 14° angle of observation. The resulting reflectance profile (dotted curve, Fig. 12, left) has a FWHM of 39.1 μm, which is an increase in the beam width that one could expect to observe, but this is not quite as much as the 62.9 μm FWHM estimated by fitting the measured data with the model.

When modeling subsurface scattering in the white resin, the black PMMA border should also be accounted for. The reflectance measured on the white resin near the border with the black PMMA is affected by the high absorption of this material in the visible range. Indeed, due to the small difference in refractive indices between the PMMA and resin, some of the scattered light is absorbed by the black PMMA, which affects our measurement at the edge of the resin dots. This effect becomes more pronounced in the case of the 100 μm dot, and it also leads to additional widening of the beam estimated by the convolution model.

Figure 12 (right) shows the results of a simulation of reflectance as measured by our instrument for an illumination beam moving across an edge between black PMMA and white resin. We can observe in this figure that, in the white resin (after 50 μm on the profile), the reflectance simulated using subsurface scattering in the resin and absorption in the PMMA (dotted curve) shows the same trend as the model fit on the measured data (solid curve), with a very slow reach of the plateau, unlike when subsurface scattering is not considered (regular dash curve). The beam FWHM estimated by our convolution model is consequently overestimated to bring the model closer to the curve simulated with subsurface scattering. In the case of a 100 μm dot, the proximity of PMMA all around the white resin attenuates the reflectance even more; the plateau is never reached, and this is likely why the BRDF measurements then fall below the model values (see Fig. 10, bottom right).

These ray tracing simulations show that better modeling of the sample can be attained considering subsurface scattering. However, these simulations rely on knowledge of the sample's optical properties. In this discussion, we decided to use values from the literature; however, many assumptions are made (for instance, the shape of the TiO_2 particles strongly impacts the anisotropy properties of the material), and the extrapolated results cannot be employed for validation purposes. Further investigations will be made in the future to better characterize the optical properties of the sample and to understand these subsurface scattering and absorption effects by realizing 2D scans of these white dots with small translation steps.

CONCLUSION

We have designed and implemented a goniospectrophotometer capable of measuring the BRDF of a surface with a measurement area of ~31 μm in diameter. We refer to this instrument as a μBRDF goniospectrophotometer. The spectral range is 380–780 nm, with a 0.9 nm spectral bandwidth. The design of the device, which can measure both the incident and reflected flux for absolute measurements of the BRDF, allows it to be traceable to the international system of units through its traceability to the meter.

Validating the system using a calibrated reflectance standard artifact (Spectralon) was not possible because, at this small scale, Spectralon is translucent, and thus, its reflectance measurement is impacted by edge-loss effects. For that reason, we developed customized samples with 100, 300, 500, and 1000 μm white dots on a black substrate to validate the system. Using a simple convolution

model, we were able to explore the measuring capabilities of the system. The μBRDF goniospectrophotometer provides values that are compatible with a measurement surface of micrometric dimensions (<100 μm) and with the expected BRDF values of the white and black areas of the test sample. Unfortunately, the non-homogeneity of the surface and the translucency of the white resin limited our demonstration.

Furthermore, our experimental measurements on the 100 μm dot revealed that μBRDF measurements are valid only when the measured sample exceeds a minimum size that depends on the translucency properties of the material. We think that there is a minimum resolution below which the BRDF quantity cannot be defined, depending on the translucency of the material. In the future, we plan to develop a new generation of samples that will avoid translucency issues and maybe provide a straightforward way to establish multi-scale traceability. We also plan to use our equipment to explore the subsurface scattering properties of dielectric materials. These works on extending the BRDF scale from centimeter to micrometer size are interesting to further the understanding of the dependence of appearance on the scale of measurement.

ACKNOWLEDGMENTS

A preliminary version of this work was presented at the CIE midterm meeting 2021 (September 27, 2021, to September 29, 2021. Hosted by MyCIE, Kuala Lumpur, Malaysia) and published in the conference proceedings.[35] The authors thank Markus Barbieri, Michele Conni, and BARBIERI electronic snc for their support of Zemax.

Part of this work is done in the frame of the ITN ApPEARS (Appearance Printing European Advanced Research School), a project funded by the European Union's Horizon 2020 program under the Marie Skłodowska–Curie Grant Agreement No. 814158. Part of this work was done in the frame of Project No. 18SIB03 BxDiff, which has received funding from the EMPIR program co-financed by the participating states and from the European Union's Horizon 2020 research and innovation program.

AUTHOR DECLARATIONS

Conflict of Interest

The authors have no conflicts to disclose.

Author Contributions

Dipanjana Saha: Conceptualization (equal); Data curation (equal); Formal analysis (equal); Investigation (equal); Methodology (equal); Project administration (equal); Resources (equal); Software (equal); Validation (equal); Visualization (equal); Writing – original draft (equal); Writing – review & editing (equal). **Lou Gevaux**: Data curation (equal); Investigation (equal); Methodology (equal); Resources (equal); Software (equal); Validation (equal); Visualization (equal); Writing – review & editing (equal). **Jeppe Revall Frisvad**: Data curation (equal); Resources (supporting); Software (equal); Supervision (supporting); Writing – review & editing (equal). **Gael Obein**: Conceptualization (equal); Funding acquisition (equal); Methodology (equal); Project administration (equal); Resources (equal); Supervision (equal); Visualization (equal); Writing – review & editing (equal).

DATA AVAILABILITY

Data underlying the results presented in this paper are not publicly available at this time but may be obtained from the corresponding author upon reasonable request.

REFERENCES

[1] T. Muller, P. Callet, F. da Graça, A. Paljic, P. Porral, and R. Hoarau, "Predictive rendering of composite materials: A multi-scale approach," Proc. SPIE **9398**, 939804 (2015).
[2] A. Luongo *et al.*, "Microstructure control in 3D printing with digital light processing," Comput. Graphics Forum **39**(1), 347–359 (2020).
[3] D. B. Judd, "Terms, definitions, and symbols in reflectometry," J. Opt. Soc. Am. **57**(4), 445–452 (1967).
[4] F. E. Nicodemus, "Directional reflectance and emissivity of an opaque surface," Appl. Opt. **4**, 767–775 (1965).
[5] G. J. Ulbrich, J. Trede, and M. Mross, "Near IR goniometer-spectrometer," Proc. SPIE **0970**, 78–85 (1989).
[6] H. W. Yoon, D. W. Allen, G. P. Eppeldauer, and B. K. Tsai, "The extension of the NIST BRDF scale from 1100 nm to 2500 nm," Proc. SPIE **7452**, 745204 (2009).
[7] G. Obein, R. Bousquet, and M. E. Nadal, "New NIST reference goniospectrometer," Proc. SPIE **5880**, 58800T (2005).
[8] A. Höpe, T. Atamas, D. Hünerhoff, S. Teichert, and K.-O. Hauer, "ARGon^3: '3D appearance robot-based gonioreflectometer' at PTB," Rev. Sci. Instrum. **83**(4), 045102 (2012).
[9] F. B. Leloup, S. Forment, P. Dutré, M. R. Pointer, and P. Hanselaer, "Design of an instrument for measuring the spectral bidirectional scatter distribution function," Appl. Opt. **47**(29), 5454–5467 (2008).
[10] G. Obein, S. Ouarets, and G. Ged, "Evaluation of the shape of the specular peak for high glossy surfaces," Proc. SPIE **9018**, 901805 (2014).
[11] M. E. Becker, "Sparkle measurement revisited: A closer look at the details," J. Soc. Inf. Disp. **23**(10), 472–485 (2015).
[12] A. Ferrero and S. Bayón, "The measurement of sparkle," Metrologia **52**(2), 317 (2015).
[13] E. Chorro *et al.*, "The minimum number of measurements for colour, sparkle, and graininess characterisation in gonio-apparent panels," Color. Technol. **131**(4), 303–309 (2015).
[14] A. Ferrero *et al.*, "Preliminary measurement scales for sparkle and graininess," Opt. Express **29**(5), 7589–7600 (2021).
[15] P. Santafé, A. Ferrero, J. Campos Acosta, and N. Tejedor-Sierra, "Primary facility for traceable measurement of the BSSRDF," Opt Express **29**(21), 34175–34188 (2021).
[16] L. Gevaux, D. Saha, and G. Obein, "Investigating the optical translucency of Spectralon using BSSRDF measurements," Appl. Opt. **62**(18), 5003–5013 (2023).
[17] JRP 18SIB03 "BxDiff" of the Euramet EMPIR program, available at https://bxdiff.cmi.cz/.
[18] F. E. Nicodemus, J. C. Richmond, J. J. Hsia, I. W. Ginsberg, and T. Limperis, "Geometrical considerations and nomenclature for reflectance," Monograph No. 160 (National Bureau of Standards, Gaithersburg, MD, 1977).
[19] A. Rabal, G. Ged, and G. Obein, "What is the true width and height of the specular peak according the level of gloss?," in *Proceedings of the 29th Quadrennial Session of the CIE* (International Commission on Illumination, CIE, 2019), p. 621.
[20] T. Labardens, P. Chavel, Y. Sortais, M. Hébert, L. Simonot, A. Rabal, and G. Obein, "Study and simulations of speckle effects on BRDF measurements at very high angular resolution," I S&T International Symposium on Electronic Imaging: Material Appearance 140–147 (2021).
[21] R. Le Breton, G. Ged, and G. Obein, "Out of plane BRDF Measurement at LNE-Cnam using 'ConDOR,' our primary goniospectrophotometer," paper presented at the Proceedings of the 28th Session of the CIE, Manchester, 2015, pp. 1401–1407.

[22]G. Obein, J. Audenaert, G. Ged, and F. B. Leloup, "Metrological issues related to BRDF measurements around the specular direction in the particular case of glossy surfaces," Proc. SPIE **9398**, 93980D (2015).
[23]T. P. Moffitt, Y.-C. Chen, and S. A. Prahl, "Preparation and characterization of polyurethane optical phantoms," J. Biomed. Opt. **11**(4), 041103 (2006).
[24]BIPM, IEC, IFCC, ILAC, ISO, IUPAC, IUPAP, and OIM, "Evaluating standard uncertainty," in *Evaluation of Measurement Data. Guide to the Expression of Uncertainty in Measurement* (Joint Committee for Guides in Metrology, JCGM, 2008).
[25]J. A. Nelder and R. Mead, "A simplex method for function minimization," Comput. J. **7**(4), 308–313 (1965).
[26]F. Alinejad, H. Bordbar, M. Makowska, and S. Hostikka, "Spectroscopic determination of the optical constants and radiative properties of black PMMA for pyrolysis modeling," Int. J. Therm. Sci. **176**, 107501 (2022).
[27]F. Alinejad, H. Bordbar, M. Makowska, and S. Hostikka, "A dataset for spectral radiative properties of black polymethyl methacrylate," Data Brief **42**, 108097 (2022).
[28]T. Siefke *et al.*, "Materials pushing the application limits of wire grid polarizers further into the deep ultraviolet spectral range," Adv. Opt. Mater. **4**(11), 1780–1786 (2016).
[29]J. Bauer *et al.*, "Determination of optical constants and scattering properties of transparent polymers for use in optoelectronics," Opt. Mater. Express **12**(1), 204–224 (2022).
[30]J. R. Frisvad, N. J. Christensen, and H. W. Jensen, "Computing the scattering properties of participating media using Lorenz-Mie theory," ACM Trans. Graphics **26**(3), 60 (2007).
[31]T. S. Trowbridge and K. P. Reitz, "Average irregularity representation of a rough surface for ray reflection," J. Opt. Soc. Am. **65**, 531–536 (1975).
[32]K. E. Torrance and E. M. Sparrow, "Theory for off-specular reflection from roughened surfaces," J. Opt. Soc. Am. **57**, 1105–1114 (1967).
[33]J. R. Frisvad *et al.*, "Predicting the appearance of materials using Lorenz–Mie theory," in *The Mie Theory*, *Springer Series in Optical Sciences*, edited by W. Hergert and T. Wriedt (Springer, Berlin, Heidelberg, 2012), Vol. 169.
[34]B. Walter *et al.*, "Microfacet models for refraction through rough surfaces," in *Proceedings of Eurographics Symposium on Rendering (EGSR'07)* (Eurographics Association, 2007), pp. 195–206.
[35]D. Saha, L. Gevaux, T. Cances, A. Richard, and G. Obein, "Development of a μBRDF goniospectrophotometer for BRDF measurement on tiny surfaces," in *CIE X048-OP42* (CIE, 2021).